

Intraband and interband relaxation of excitonic polaritons

A. B. Pevtsov, A. V. Sel'kin, N. N. Syrbu, and A. G. Umanets

A. F. Ioffe Physicotechnical Institute, Academy of Sciences of the USSR, Leningrad

(Submitted 17 April 1985)

Zh. Eksp. Teor. Fiz. **89**, 1155–1167 (October 1985)

A well-defined doublet structure due to polariton emission has been found in the spectra of resonance exciton luminescence emitted by the black modification of ZnP_2 crystals at $T = 2$ K. The shape of the spectra is analyzed on the basis of the theory of spectral and spatial diffusion of polaritons under boundary conditions consistent with experimental reflection data. The relative contributions of polaritons belonging to the upper (UBP) and lower (LBP) dispersion branches are determined for the first time. It is shown that the UBP contribution to the emitted radiation depends significantly on the rate of interband UBP→LBP relaxation and the LBP spatial and energy distribution. The LBP distribution function is largely established as a result of intraband relaxation between LBP states. The ratio of LBP to UBP emission intensities is used to determine the effective depth of the LBP spatial distribution.

§1. INTRODUCTION

Polariton effects play an important role in the emission spectra of crystals in the neighborhood of exciton resonances.¹ There is a whole range of spectroscopic and temporal features of exciton luminescence that can be explained in terms of polariton theory.^{1–6} The basic qualitative aspects of the phenomenon of polariton luminescence (PL) due to polariton dispersion, the transmission of radiation through the crystal boundary in the region of resonance, and the nature of the spatial and energy distributions of polaritons have frequently been discussed (see, for example, Ref. 7 and the literature cited therein). However, a sufficiently rigorous quantitative analysis of specific experimental data has been lacking.

It has not been entirely clear which polariton state (upper or lower branch) provides the principal contribution to the short-wave wing of the PL spectrum and what are the manifestations of the spatial distribution of polaritons. More experimental attention will have to be devoted to the true effect of the crystal boundary (as part of the problem of additional boundary conditions (ABC)⁸ and the problem of taking into account surface states⁹). There is considerable interest in the energy relaxation of polaritons under the conditions of their strong spatial diffusion.¹⁰

Practical analysis of PL spectra has mostly been confined to two approaches. One is based on the solution of the simplified transport equation in which the collision integral, or part of it, is replaced by an empirical expression selected on the basis of qualitative considerations.^{2,7,11–13} The range of validity of this method of analysis is still to be elucidated. The other approach, in which the collision integral is evaluated explicitly,^{3,5,6,10,14} seems more rigorous.

We shall use the second approach to analyze, within the framework of the theory of spectral and spatial diffusion of polaritons, the spectra of resonance exciton luminescence of the black modification of ZnP_2 crystals. These crystals have a number of interesting and nontrivial properties near the fundamental absorption edge,^{15,16} among which we note the abundant hydrogen-like spectrum of exciton states (up to

the state with principal quantum number¹⁵ $n = 7$). The lowest-lying $n = 1$ exciton state of these crystals (which have rhombic macrosymmetry) is characterized by large longitudinal-transverse splitting, the effective mass of the exciton is not very much greater than the mass of the free electron, and the luminescence spectra contain well-defined features characteristic of the polariton emission mechanism. All this enables us to look upon rhombic ZnP_2 crystals as very convenient model objects for the detailed investigation of excitonic polaritons, including features due to additional waves.

We shall devote particular attention to the relative contribution to the external emission due to polaritons in the upper and lower dispersion branches (UBP and LBP, respectively). Since the solution of this problem is closely related to the analysis of ABC, we shall, in Section 2, perform a comprehensive investigation of the amplitude and phase reflection spectra of ZnP_2 crystals for different angles of incidence. We shall also determine the values of all the parameters necessary to construct the polariton dispersion curves. The experimental data on luminescence, given in Section 2, are analyzed in Section 4 in terms of the theory of spectral and spatial diffusion of polaritons, an account of which is given in Section 3. The analysis takes into account the boundary conditions corresponding to the experimental reflection data.

§2. EXPERIMENTAL RESULTS. DETERMINATION OF THE POLARITON DISPERSION PARAMETERS

We have investigated single-crystal ZnP_2 plates grown by the gas-transport method.¹⁵ The dimensions and the quality of the natural faces of the crystals enabled us to record reliably both the specular reflection spectra and the luminescence spectra. The experimental geometry was chosen so that the C_{2z} twofold axis of the crystal, lying along the dipole moment vector of the exciton under consideration (nondegenerate state), was parallel to the reflecting (or radiating) face, with light propagating along $\mathbf{K} \perp C_{2z}$. The crystal thickness was 0.1–1 mm, so that the back face had no effect on the results. The measurements were performed for

different angles φ between the direction of propagation of the recorded light and the normal to the face of the crystal.

The optical spectra were investigated at $T = 2$ K (the crystals were placed directly in pumped-off liquid helium) in a system based on the DFS-24 spectrometer. The spectral width of the spectrometer slits was 0.05 meV at $\varphi \approx 0^\circ$ and 0.1 meV at $\varphi > 70^\circ$. Luminescence was excited by the Kr^+ laser at 6471 Å, using pump power not exceeding 500 mW within the 0.5-mm diameter light spot. The reflected light was investigated using the continuous spectrum of an incandescent lamp.

The polariton luminescence spectrum is largely determined by the polariton dispersion parameters. To construct the polariton dispersion curves, we first followed the method of Ref. 17 and investigated the amplitude-phase exciton reflection spectra of ZnP_2 crystals at different angles of incidence φ . We directly measured the energy reflection coefficients $R_\delta(\psi_0, \varphi, \psi)$, where ψ_0 and ψ are the azimuthal angles of the polarizer and analyzer, φ is the angle of incidence, and δ is the additional phase shift (between the p - and s -amplitudes of the reflected light) introduced by a phase-shifting wedge. The angles ψ_0 and ψ were measured from the plane of incidence (perpendicular to the C_{2z} axis), using the right-hand rule with the screw axis pointing in the direction of propagation.

Figure 1 ($a_i, b_i, c_i; i = 1, \dots, 4$; the points are experimental) shows the reflection spectra $R_\delta(\psi_0, \varphi, \psi)$ and the spectra of the phase shift $\Delta = \Delta_p - \Delta_s$ between the p - and s -

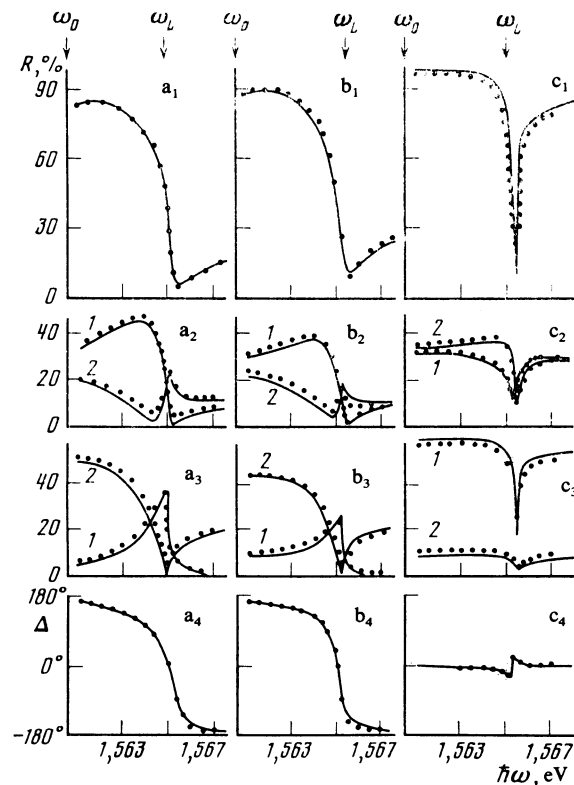


FIG. 1. Amplitude-phase exciton reflection spectra of ZnP_2 crystals at $T = 2$ K (see text for explanation).

amplitudes of the reflected wave for angles of incidence $\varphi = 8^\circ$ (a), 65° (b), 85° (c): $\psi_0 = \psi = 90^\circ$ ($i = 1$), $\psi_0 = -\psi = 45^\circ$ ($i = 2, 3$ -curves 2), $\psi_0 = \psi = 45^\circ$ ($i = 2, 3$ -curves 1), $\delta = -\pi/2$ ($i = 2$), $\delta = 0$ ($i = 3$). The phase shift Δ was calculated from the $i = 2, 3$ spectra (see Ref. 17).

The measured spectra were analyzed within the framework of the theory of additional light waves,¹⁸ which takes into account the exciton-free ("dead") layer on the crystal boundary.¹⁹ The best agreement between the theory (solid curves in Fig. 1) and experiment was achieved for the following parameters of the theoretical model: resonance frequency $\omega_0 = 1.5606$ eV, longitudinal-transverse splitting $\omega_{LT} = 4.5$ meV, effective exciton mass (in units of the free electron mass) $M = 3$, phonon permittivity $\epsilon_0 = 12$, damping parameter $\Gamma = 0.1$ meV, and dead layer thickness $l = 60$ Å.

We note that the ordinary reflection spectrum of ZnP_2 at near-normal incidence (Fig. 1, a_1 , s -polarization) does not contain near the reflection minimum any sharp anomalies (such as the spike observed for CdS in Ref. 19) which could be effectively exploited to identify the longitudinal frequency $\omega_L = \omega_0 + \omega_{LT}$. On the other hand, it is clear from Fig. 1 that, by increasing the angle of incidence or by varying the azimuths ψ_0, ψ and the phase shift δ , we could ensure the appearance of such anomalies and thereby more reliably deduce the polariton energy spectrum.

The spectra of the phase Δ carry independent (as compared with the ordinary reflection spectra) information that can be used to verify the validity of the chosen model. For example, the variation in the shape of the phase spectrum (see b_4 and c_4) with increasing φ is a qualitative manifestation of the Brewster exciton effect, which can be naturally explained²⁰ on the basis of the above model.

The luminescence spectra of ZnP_2 crystals were recorded for the same points on the crystal surface as the reflection spectra because we needed the closest possible comparison of the spectra. Figure 2 shows the polariton emission spectra of ZnP_2 , recorded at emission angles $\varphi = 0^\circ$ (a) and $\varphi = 76^\circ$

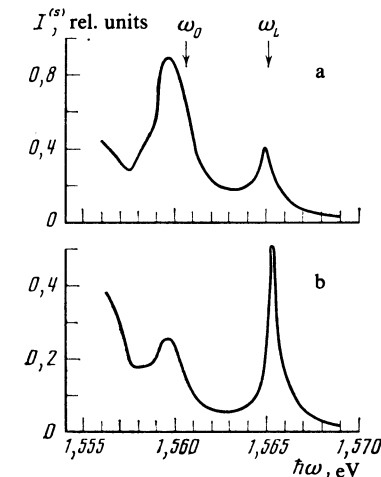


FIG. 2. Polariton luminescence spectra of ZnP_2 crystals at $T = 2$ K, recorded at different angles φ of emission relative to the normal to the surface: a— $\varphi = 0^\circ$, b— $\varphi = 76^\circ$.

(b) for $E||C_{2z}$ polarization. The vertical arrows mark the frequencies ω_0 and ω_L . The ordinate is the radiation intensity in relative units which are the same in both Figs. 1a and 1b (the relative normalization of the spectra a and b is discussed below).

On the long-wave side of the PL bands in Fig. 2, there is a number of strong emission lines (not reproduced here), which can be ascribed to bound exciton states. We have not been able to identify clearly emission features due to phonon replicas.

It is clear from Fig. 2 that the PL spectrum of ZnP_2 has a well-defined doublet structure. A substantial modification of the spectrum occurs as the emission angle is varied (at constant polarization $E||C_{2z}$): the short-wave component of the doublet becomes appreciably narrower and stronger as compared with the long-wave component. The details of the PL spectrum of ZnP_2 were reproduced with record-breaking resolution (for semiconducting crystals) because of the high value of ω_{LT} and low values of Γ . The analysis of the ZnP_2 spectra can therefore be performed in greater detail as compared with the spectra of other known semiconducting crystals.

§3. SPECTRAL AND SPATIAL DIFFUSION OF POLARITONS

In the polariton mechanism, the emission of light by the crystal is looked upon as the transformation of a polariton, incident from the interior of the crystal on its face, into an external photon.¹ The probability of this transformation is determined by the intensity transmission coefficients of the crystal faces.^{21,22} This approach implies that we can use the Boltzmann transport equation for the polariton distribution function $f_j^{(\lambda)}(\mathbf{K}, \mathbf{r}, t)$, which depends on the wave vector \mathbf{K} of the polariton, its position vector \mathbf{r} , and the time t (j is the polariton branch number and λ is the polarization index). The quantity $f_j^{(\lambda)}(\mathbf{K}, \mathbf{r}, t) d^3\mathbf{K} d^3\mathbf{r}$ is the number of polaritons in the volume element $d^3\mathbf{K} d^3\mathbf{r}$ of phase space at the point \mathbf{K}, \mathbf{r} at time t .

The set of transport equations for the functions $f_j^{(\lambda)}$ will be considered in the simplest case of the isolated dipole-active exciton resonance in a cubic crystal, neglecting the contribution of longitudinal excitons, i.e., confining our attention to the two-band model ($j = 1, 2$). The dependence of the polariton frequency ω on the wave vector \mathbf{K} then has the well-known form shown in Fig. 3, where the solid curves 1 and 2 represent the lower and upper dispersion branches, respectively. The dot-dash curve marks the band of mechanical excitons⁸ that would characterize the spectrum of intrinsic excitations of the crystal in the absence of the light-exciton interaction.

In view of the above experimental data, we are interested in time-independent polariton luminescence in a spectral interval of the order of $3\omega_{LT} - 4\omega_{LT}$, which includes the region of longitudinal-transverse splitting. We shall assume that the collision integral includes a contribution due to inelastic scattering of polaritons, assisted by longitudinal acoustic (LA) phonons,³ and a contribution due to elastic scattering (R) by defects and impurities (these processes are illustrated schematically by the dashed curves in Fig. 3).

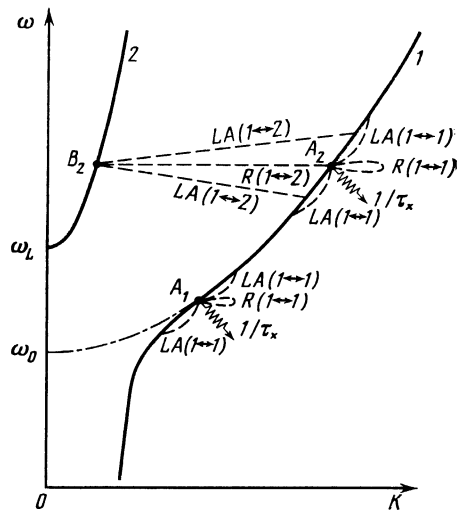


FIG. 3. Polariton dispersion curves corresponding to the lower (1) and upper (2) branches. Dashed curves illustrate schematically the inelastic scattering of polaritons by longitudinal acoustic (LA) phonons and the elastic scattering (R) by defects or impurities. $1/\tau_x$ corresponds to the radiationless loss of a polariton.

Moreover, we shall take into account the following points:

(a) the spectral density of states on branch 1 is relatively high, so that multiple intraband ($1 \leftrightarrow 1$) scattering of polaritons occurs on this branch in such a way that the distribution function $f_1^{(\lambda)}$ becomes almost isotropic and independent of the polariton polarization index λ ;

(b) the density of states on branch 2 is low, so that intraband scattering of the form $2 \leftrightarrow 2$ is relatively unimportant, i.e., the population of the polariton states on branch 2 is largely determined by single interband scattering of the form $1 \rightarrow 2$.

Under these assumptions, the transport equation for LBP may be considered independently of the equation for branch 2, and integration over the directions of propagation (for example, as in radiation transfer theory²³) reduces to the diffusion-type equation

$$D\Delta f_1 - f_1/\tau_x + G + \hat{Q}f_1 = 0, \quad (1)$$

where f_1 is the isotropic part of the LBP distribution function, $D = (\frac{1}{3})v_1^2 \tau_p$ is the diffusion coefficient (not averaged over the energy distribution), which depends on frequency through the group velocity v_1 , the momentum relaxation time is $\tau_p = (1/\tau_{ac} + 1/\tau_{el})^{-1}$, τ_{ac} and τ_{el} are the relaxation times associated, respectively, with elastic scattering by LA phonons and elastic scattering by impurities and defects, τ_x is the lifetime for the radiationless annihilation of the polariton, G is the source function averaged over the directions of emission, and \hat{Q} is the inelastic collision operator, defined to within second-order corrections in the parameter $u/v_1 \ll 1$ (u is the velocity of sound and v_1 is the LBP group velocity),¹⁴

$$\hat{Q}f_1 = \frac{2}{3} \frac{(E_c - E_v)^2}{\pi \rho \hbar} \frac{v_1}{K_1^2} \frac{d}{d\omega} \times \left\{ \frac{K_1^6}{v_1^2} \left[1 + \left(\frac{86}{105} u K_1 + \frac{T}{\hbar} \right) \frac{d}{d\omega} \right] f_1(K_1(\omega), \mathbf{r}) \right\}. \quad (2)$$

Moreover, E_c and E_v are the deformation-potential constants for the conduction and valence bands, respectively, ρ is the density of the crystal, and T is the temperature in energy units. In deriving (2), the temperature dependence of the phonon occupation number N_q (q is the phonon wave number) was approximated by the linear function $N_q \simeq T/\hbar u q$, which gives the correct result for $T \simeq 0$ and $T \gg \hbar u q$.

In the coordinate frame in which the y axis points inward into a semi-infinite crystal, and is perpendicular to its $y = 0$ face, the boundary condition for (1), which expresses the energy balance on the surface, assumes the form

$$\left(D \frac{\partial f_1}{\partial y} - \gamma_s f_1 \right) \Big|_{y=0} = 0, \quad (3)$$

where γ_s is the rate of surface annihilation of polaritons (including transmission and reflection effects and radiationless loss on the surface). Moreover, $f_1(K_1(\omega), y)|_{y=\infty} = 0$.

The above second-order partial differential equation (in spatial coordinates and frequency) describes the spectral and spatial LBP diffusion. This type of equation was solved in Ref. 10 for the PL spectrum of an anisotropic crystal plate, using a special source function G (δ taken to be a function of ω and y ; resonance excitation) and particular boundary conditions for frequency.

Under the conditions of our experiment, the pump frequency was much greater than the frequency corresponding to the fundamental absorption edge. We may therefore suppose that the spatial LBP distribution was established mainly outside the spectral range of the emission. When the depth of the distribution is large enough, energy relaxation of polaritons in the relatively narrow region of longitudinal-transverse splitting should not produce a significant change in the nature of the spatial distribution (the crystal boundary has an appreciable effect only for $\omega < \omega_0$ because of the rapid increase in the rate of radiative surface annihilation of polaritons, which is mainly inversely proportional to the spectral density of states).

The distribution function $f_1(K_1(\omega), y)$ can then be factorized with respect to the variables ω and y by specifying the spatial part f_1 in the approximate form $\sim \exp(-y/L)$, where L is the effective depth of the distribution. Assuming that $G = 0$ in the emission region, and integrating (1) with respect to y between 0 and ∞ , subject to the above boundary conditions, we obtain

$$Q f_1 - \Gamma_{xs} f_1 = 0, \quad (4)$$

where $\Gamma_{xs} = 1/\tau_x + \gamma_s/L$ is the total reciprocal polariton lifetime in band 1 (lower branch).

The last equation is actually the differential form of the balance equation for the number of polaritons (compare this with Refs. 3 and 14). However, in contrast to Refs. 3 and 14, it takes into account the inhomogeneity of the spatial distribution of polaritons by introducing the effective distribution depth L (the thickness of the crystal plate is used in Ref. 3 instead of L). It is clear from (4) that, in this approximation, we cannot separate the probability of radiationless decay within the bulk of the specimen from the probability of surface annihilation.

The solution of (4) under particular boundary conditions for the frequency enables us to find the frequency dependence of the LBP distribution function $f_1(K_1(\omega), y)$. The UBP distribution function $f_2(\mathbf{K}_2, y)$ satisfies the following transport equation under the above assumptions:

$$v_{2y} \frac{\partial f_2}{\partial y} = -\Gamma_{12} f_2 + \sum_{\mathbf{K}_1', h} W_{21}^{(h)}(\mathbf{K}_2, \mathbf{K}_1') f_1(K_1', y), \quad (5)$$

where

$$\Gamma_{12} = \sum_{\mathbf{K}_1', h} W_{12}^{(h)}(\mathbf{K}_1', \mathbf{K}_2)$$

is the reciprocal UBP lifetime due to interband scattering to the LBP state and $W_{ji}^{(h)}(\mathbf{K}_j, \mathbf{K}_i')$ is the probability of scattering of a polariton from the state $|\mathbf{K}_i'\rangle$ to the state $|\mathbf{K}_j\rangle$ as a result of the h -type mechanism. The radiationless lifetime τ_x does not appear in (5) because, in the approximation in which the diffusion equation (1) is valid, we have $\Gamma_{12} \gg \tau_x^{-1}$, where

$$\Gamma_{12} \approx \Gamma_{11} = \sum_{\mathbf{K}_1', h} W_{11}^{(h)}(\mathbf{K}_1', \mathbf{K}_1).$$

If we neglect the inelastic interband scattering of polaritons by LA phonons, the solution of (5) for polaritons propagating toward the boundary of the crystal ($v_{2y} < 0$) assumes the simple form

$$f_2^-(\mathbf{K}_2, y) = \frac{L \Gamma_{12}}{|v_{2y}| + L \Gamma_{12}} f_1(K_1, y). \quad (6)$$

It is clear from this that the function f_2^- is determined not only by the probability of interband scattering (through Γ_{12}), but also by the effect of the depth L . In general, f_2^- is then anisotropic despite the isotropic nature of the interband scattering ($K_2 \ll K_1$). This anisotropy appears because the denominator of (6) contains the component of the velocity v_2 in the direction of the normal to the crystal surface and, in the final analysis, is due to the inhomogeneity of the spatial LBP distribution.

The final solution of the emission problem is determined by the connection between the intensity of external emission and the boundary values of the distribution functions $f_j(\mathbf{K}_j, +0)$. If $I^{(\lambda)}(\omega, \varphi)$ is the spectral density of the intensity escaping from the crystal with λ polarization ($\lambda = s, p$), then

$$I^{(\lambda)}(\omega, \varphi) = \frac{\hbar \omega^3}{c^2} \sum_j T_j^{(\lambda)}(\omega, \varphi) f_j(\mathbf{K}_j, +0), \quad (7)$$

where φ is the angle of emission, $T_j^{(\lambda)}$ is the energy transmission coefficient of the crystal face in the crystal \rightarrow vacuum direction for λ -polarized detected external light, and c is the velocity of light in vacuum. The orientation of the vector \mathbf{K}_j relative to the direction of emission is determined by the usual laws of refraction at the crystal surface.

§4. ANALYSIS OF EXPERIMENTAL RESULTS. RELATIVE CONTRIBUTION OF THE UPPER AND LOWER BRANCHES TO POLARITON EMISSION

In the analysis of experimental emission spectra, we shall allow for the fact that the principal contribution to

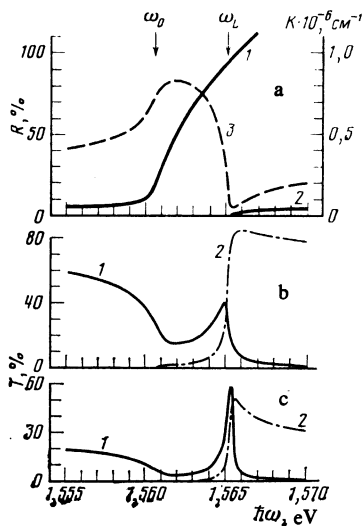


FIG. 4. Theoretical energy dependence of the reflection (a—dashed curve) and the transmission (b,c) coefficients of the crystal surface for angles of incidence $\varphi = 0^\circ$ (a,b) and $\varphi = 76^\circ$ (c): 1—LBP, 2—UBP (the corresponding polariton dispersion curves are shown in Fig. 8 by the solid lines 1 and 2). Parameter values corresponding to the experimental data on reflection (Fig. 1) were used in the calculations.

emission for $\omega < \omega_L$ is provided for LBP. The wavelength dependence of the function f_1 in this region can then be determined by dividing the observed luminescence spectrum $I^{(\lambda)}(\omega, \varphi)$ by $T_1^{(\lambda)}(\omega, \varphi)$, and then extrapolating to the region $\omega > \omega_L$ with the aid of the spectral diffusion equation (4). The function f_2 can then be calculated from the transport equation (5), and formula (7) can be used to compare the theoretical results with experimental data.

Following this program, we present in Fig. 4 the calculated polariton dispersion curves (a, curves 1 and 2), the reflection coefficient $R^{(s)}(\omega, \varphi)$ (a, curve 3, $\varphi = 0^\circ$), and the transmission coefficient $T_{1,2}^{(s)}(\omega, \varphi)$ (b, curves 1, 2, $\varphi = 0^\circ$; c, curves 1, 2, $\varphi = 76^\circ$). The coefficients were calculated for radiation entering the crystal from vacuum, using the dead-layer model employed in the analysis of reflection spectra. In the reverse case of emission of radiation from the crystal, these coefficients will have the same values provided only that absorption is low enough. This reversibility follows from the symmetry of the system under time reversal.²²

The condition that absorption must be low will also determine the range of validity of the transport equation: the polariton wavelength must not, at any rate, exceed its mean free path. For the resulting values of the damping parameter Γ , this condition breaks down only near the point $K = 0$, i.e., for branch 2 polaritons near the frequency ω_L . Nevertheless, the coefficient $T_2^{(s)}$ still retains its macroscopic meaning (as the ratio of the energy fluxes) even for $\omega \lesssim \omega_L$, where $T_2^{(s)} \neq 0$ for $\Gamma \neq 0$ (Ref. 21); see Figs. 4b and c, curves 2.

Figure 5 shows the results obtained by dividing the spectra observed at two different angles of emission (see Fig. 2) by the corresponding transmission coefficients $T_1^{(s)}(\omega, \varphi)$: dark circles $\varphi = 0^\circ$, open circles $\varphi = 76^\circ$. It may be considered that, for $\omega < \omega_L$ (with the exception of a small

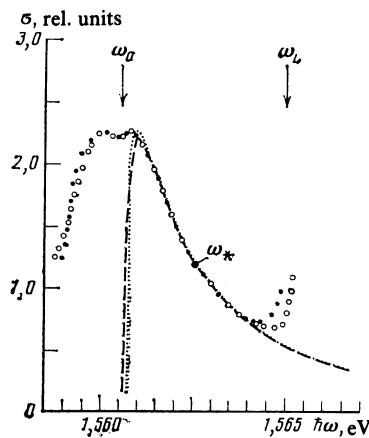


FIG. 5. Energy dependence of the ratio $\sigma(\omega, \varphi) = I^{(s)}(\omega, \varphi) / T_1^{(s)}(\omega, \varphi)$ of the intensity $I^{(s)}$ of external emission to the transmission coefficient $T^{(s)}$ for emission angles $\varphi = 0^\circ$ (dark circles) and $\varphi = 76^\circ$ (open circles). The dashed and dotted curves were obtained by numerical solution of (5) on the assumption of parabolic polariton dispersion for $\omega > \omega_0$ in the case of three-dimensional and two-dimensional migration, respectively. ω_* is the frequency at which the frequency boundary conditions were specified for the distribution function $f_1 = \sigma$ and its derivative $\partial f_1 / \partial \omega = d\sigma / d\omega$.

region on the long-wave side of ω_L), the ratio $\sigma(\omega, \varphi) = I^{(s)}(\omega, \varphi) / T_1^{(s)}(\omega, \varphi)$ reproduces the spectral dependence of the function $f_1(K_1(\omega), +0)$, since states corresponding to branch 2 do not participate in emission in this spectral region ($T_2^{(s)}, f_2 \approx 0$), and the factor in front of the sum in (7) does not vary appreciably for $|\omega - \omega_0| \ll \omega_0$. Moreover, the quantity $\sigma(\omega, \varphi)$ should not be very dependent on the angle φ , even if f_1 is an anisotropic function: because of the high refractive index $n_1 = cK_1/\omega$ for $\omega \gtrsim \omega_0$, the LBP contributing to emission propagates practically along the normal within the small solid angle $2\pi/n_1^2 \ll 1$.

The latter fact enables us to look upon the equation $\sigma(\omega, 0^\circ) = \sigma(\omega, 76^\circ)$ in the frequency range $\omega_0 \lesssim \omega < \omega_L$ as the natural condition for the relative normalization of spectra a and b in Fig. 2. The $\sigma(\omega, f)$ curves are in good agreement in the spectral range $1.5590 < \omega < 1.5640$ eV which contains the resonance frequency ω_0 . The two curves exhibit a small dip near ω_0 . This dip is not present in the original emission spectra. Both curves bend upward on the short-wave side, and become appreciably different.

The difference between the $\sigma(\omega, 0^\circ)$ and $\sigma(\omega, 76^\circ)$ curves in the short-wave part of the spectrum shows that there is a contribution to the UBP emission that depends appreciably on the angle of emission near the frequency ω_L because of the strong angular dependence of the coefficients $T_2^{(s)}(\omega, \varphi)$. At the same time, it is noticeable that the UBP emission occurs for $\omega < \omega_L$, as well.

The doublet structure of the peak of the distribution function $f_1(K_1, +0) = \sigma(\omega, \varphi)$ is probably due to the scattering of polaritons (with the emission of LA phonons) from the region corresponding to the short-wave component of the doublet, whilst the probability of radiative escape of polaritons decreases rapidly toward longer wavelengths (compare this with the situation in anthracene crystals²⁴). Thus,

the long-wave component of the doublet peak of the distribution function must be looked upon as a "phonon replica" (on the LA phonon) of the primary short-wave component. Here, we draw attention to the fact that, in the ZnP_2 crystals under consideration, the minimum group velocity of the polariton is $v_{1\text{min}} \simeq 9.1 \times 10^5$ cm/s, which is only slightly greater than the longitudinal sound velocity²⁵ $u \simeq 6.1 \times 10^5$ cm/s.

In view of these velocity values, the second approximation in the parameter u/v_1 in the inelastic collision operator (2) may not be sufficient near ω_0 . In the quantitative analysis of the shape of the luminescence spectrum, we therefore used (4) only in the region of parabolic dispersion of branch 1 polaritons ($\omega > \omega_0$). The frequency boundary conditions were taken to be the experimental values of the function f_1 and its derivative $\partial f_1/\partial\omega$ at the point $\omega_* = 1.5626$ eV (see Fig. 5), which lies in the region of the longitudinal-transverse splitting. The only adjustable parameter was the ratio $\eta(\omega) = \Gamma_{xs}/a_0(\omega)$, where $a_0(\omega) \simeq 5u/[v_1(\omega)\tau_{ac}(\omega)]$ is the coefficient of the zero-order derivative in the differential operator \hat{Q} (the case $T = 0$ K). By varying $\eta(\omega)$ at the frequency ω_L , the solutions of (5) were fitted to the experimental $\sigma(\omega, \varphi)$ curve in a widest possible spectral range. The best agreement was achieved for $\eta(\omega_L) = 0.14$ (dashed curve in Fig. 5).

However, it is important to remember that the investigated exciton state of ZnP_2 is nondegenerate. Polariton migration into the $\omega < \omega_L$ region is therefore largely two-dimensional in character.²⁶ The use of the three-dimensional relaxation model is then not entirely correct. The solution of (4), with the operator \hat{Q} corresponding to the limiting case of two-dimensional polariton relaxation (in the plane perpendicular to the C_{2z} axis of the crystal), is shown by the dotted curve in Fig. 5. The optimum value $\eta = 0.01 \ll 1$, obtained in this case, shows, on the one hand, that there is no radiationless surface annihilation of polaritons, which is in agreement with the set of boundary conditions used to calculate the reflection and transmission coefficients. On the other hand, this low value of η suggests that the polariton lifetime in band 1 is very small in comparison with τ_{ac} , which confirms that the diffusion approximation can be used. Comparison of the dotted and dashed curves shows that extrapolation to the $\omega > \omega_L$ region in the equations of two-dimensional and three-dimensional relaxation yields practically the same results (with the exception of the value of η and, consequently, Γ_{xs}). As far as the radiative loss of polaritons due to transmission by the boundary is concerned, such processes do not provide an appreciable contribution to Γ_{xs} for $\omega > \omega_0$. This is due, on the one hand, to the relatively low velocity v_1 of exciton-like polaritons and, on the other, the high refractive index n_1 , which defines a very small internal solid angle from which the LBP can be emitted in the upward direction. Because of the effect of the small solid angle within which the LBP propagate, and are scattered by internal reflection to the UBP states, it is found that surface-induced reabsorption is also unimportant⁴ for the ZnP_2 parameters (for $\omega > \omega_L$).

The contribution of branch 1 polariton intensity $I_1^{(s)}$ to the external emission intensity $I^{(s)}$ was determined from the

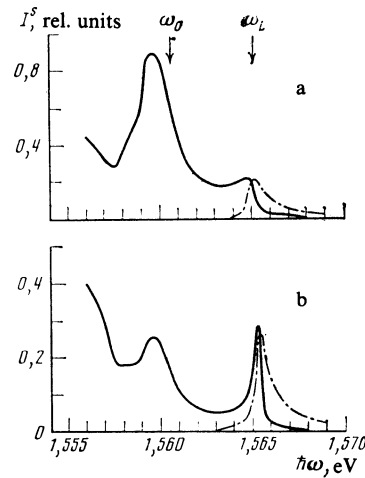


FIG. 6. Partial contributions $I_1^{(s)}$ (solid curves) and $I_2^{(s)}$ (dot-dash curves) to the external UBP and LBP emission intensity, respectively, determined from the calculated LBP distribution function: a— $\varphi = 0^\circ$, b— $\varphi = 76^\circ$.

extrapolated function f_1 with the aid of formula (7), and the experimental data of Fig. 2 were then used to extract the corresponding branch 2 contribution: $I_2^{(s)} = I^{(s)} - I_1^{(s)}$. Figure 6 shows the energy dependence of the intensities $I_1^{(s)}$ and $I_2^{(s)}$. It is clear that the contributions of the UBP and LBP states to emission near the longitudinal frequency ω_L are comparable.

Figure 7 shows, on a larger scale, the short-wave wings of the function $f_2 = f_2^-$ that provide a contribution to the external emission at $\varphi = 0^\circ$ (full points) and $\varphi = 76^\circ$ (open circles). The energy dependence of the function f_2^- ($\mathbf{K}_2, +0$) was constructed by dividing the partial intensities $I_2^{(s)}$ (see Fig. 6) by the transmission coefficients $T_2^{(s)}(\omega, \varphi)$. It is clear that this construction is justified for frequencies where the transport equation can be used for the UBP, i.e., for $\omega > \omega_L$, provided the emission angles φ are small and $\omega > \omega_1$ ($n_2(\omega_1) = 1$) for the maximum possible φ .

The appearance of branch-2 radiating states on the long-wave side of ω_L and ω_1 in the spectra (Fig. 6) is due to

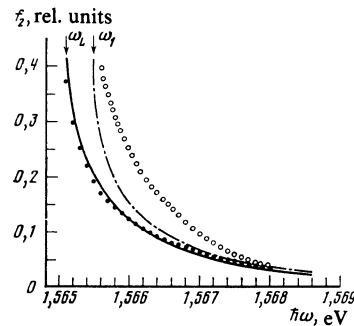


FIG. 7. UBP distribution contributing to external emission at the following angles of emission: dark circles— $\varphi = 0^\circ$, open circles— $\varphi = 76^\circ$. The solid and dot-dash curves were calculated from (7) for the same values of φ , and ω_1 is the frequency at which the UBP refractive index is equal to unity.

the uncertainty in the wave vector of these states near ω_L, ω_1 when the reciprocal lifetime Γ_{12} is finite. When $\Gamma_{12} \neq 0$, the conservation of momentum in $1 \rightarrow 2$ type scattering is not exact, which leads to interband transitions into the region $\omega < \omega_L, \omega_1$. As Γ_{12} increases, there is also a marked rearrangement of the spectrum of type 2 normal waves near ω_L . It is precisely for this reason that Γ_{12} determines the character of the reflection spectrum in the region of the minimum reflection coefficient, and the value of the phenomenological parameter Γ determined from the reflection spectra is equal to Γ_{12} in the neighborhood of ω_L .

Substituting $\Gamma_{12} = \Gamma = 0.1$ meV (see Section 2) in (6), and using the experimental data for $f_1 = \sigma$ (Fig. 5) and f_2^- (Fig. 7), we can estimate the effective depth L of the distribution of branch 1 polaritons. Thus, for $L = 5.4 \mu\text{m}$, the function f_2^- calculated from (6) for $\varphi = 0^\circ$ (solid curve in Fig. 7) is in good agreement with the corresponding experimental dependence. For $\varphi = 76^\circ$, and the same value of L , there is a discrepancy between the theoretical (dashed lines) and experimental curves, although the character of the anisotropy of f_2^- predicted by (6) is reproduced. This discrepancy may be due to an inadequate approximation to the spatial LBP distribution and the possible coordinate dependence of the parameter Γ .

A further uncertainty in the theoretical results may be due to the neglect of relaxation over the states of mixed polariton modes (including longitudinal excitons) in the region $\omega > \omega_L$. However, in our case, the frequency ω is not too far from ω_L ($\omega - \omega_L \lesssim 0.7 \omega_{LT}$) and the spectral density of states $g(\omega, \theta)$ per unit solid angle is still a rapidly-varying function of the angle θ between the optical axis of the crystal and the polariton wave vector. The maximum value of $g(\omega, \theta)$ at constant frequency is achieved for $\theta = \pi/2$, i.e., for a state with maximum $|\mathbf{K}|$. Moreover, the square of the modulus of the matrix element in the probability of scattering of a polariton by an LA phonon between states with wave vectors \mathbf{K} and \mathbf{K}' is a linear function of the difference³ $q = |\mathbf{K}' - \mathbf{K}|$, i.e., it becomes a maximum for the maximum possible (allowed by energy-momentum conservation) values of $|\mathbf{K}|$ and $|\mathbf{K}'|$. It may therefore be considered that, in this frequency range, polariton relaxation proceeds largely over the states of transverse (or almost transverse) polaritons that have maximum wave vectors. The two-band polariton relaxation model is therefore completely justified for a cubic crystal (it does not take into account the contribution of longitudinal excitons; see Section 3) provided only the ratio $(\omega - \omega_L)/\omega_{LT}$ is low enough.

§5. CONCLUSION

Our investigation of the resonance exciton luminescence spectra of ZnP_2 crystals has enabled us to identify the most essential features of the polariton emission spectra. Owing to the unique (from the point of view of polariton effects) properties of these crystals, we were able, for the first time, to analyze reliably the relative UBP and LBP contributions to the external emission. The experimental data presented above were then used to show that the emission near the longitudinal frequency ω_L was due to polaritons

belonging to both branches, i.e., both upper and lower. The shape of the spectrum and the intensity of this emission is determined by the spatial and energy distribution of the LBP and the probability of interband scattering of the LBP to UBP states.

The nature of the boundary conditions, which determine the energy dependence of the transmission coefficients of the crystal boundary, plays an important role in the formation of the polariton luminescence spectrum. The influence of these coefficients can be clearly seen in the strong dependence of the shape of the luminescence spectrum on the angle of emission of radiation by the crystal. A composite analysis of the amplitude and phase reflection spectra has yielded the boundary conditions that are in good agreement with experimental data on reflection. These boundary conditions were subsequently used to calculate the transmission coefficients and reproduce the polariton distribution function on the crystal boundary.

The frequency dependence of the LBP distribution function was analyzed within the framework of the diffusion approximation, and the boundary conditions established in the above way enabled us to conclude that radiationless surface annihilation of volume polaritons does not play a significant role in these crystals. As far as exciton surface states are concerned, which may also affect the resonance luminescence spectra of crystals,⁹ they are simply not formed in our case because the radiating surface is parallel to the optical axis of the crystal and the exciton transition is polarized along this axis.²⁶

The spatial and energy relaxation of polaritons has a diffusion character in our specimens. The effective depth of the spatial distribution of polaritons determined from the ratio of the LBP to UBP emission intensities is then 5–6 μm at $T = 2$ K. Because of the small internal solid angles in which outwardly radiating polaritons propagate, the probability of their radiative escape is small for $\omega > \omega_0$. Since radiationless surface annihilation is also unimportant, it may be considered that the diffusion flux of polaritons is practically zero on the crystal boundary for $\omega > \omega_0$. For $\omega < \omega_0$, the principal effect on the polariton luminescence spectrum is due to the radiative escape of polaritons through the boundary and intensive diffusion into the interior of the specimen.

Although our main results were obtained for particular samples, namely, zinc diphosphide crystals, their consequences and our conclusions are more general and can be used to interpret polariton luminescence spectra of other crystals.

The authors are grateful to E. L. Ivchenko and S. A. Permogorov for useful discussions.

¹V. M. Agranovich and M. D. Galanin, *Perenos energii elektronogo vzbuzhdeniya v kondensirovannykh sredakh* (Transport of Electronic Excitation Energy in Condensed Media), Nauka, Moscow, 1978, Chap. 4, Sec. 11.

²W. C. Tait and R. L. Weiher, *Phys. Rev.* **178**, 1404 (1969).

³H. Sumi, *J. Phys. Soc. Jpn.* **41**, 526 (1976).

⁴V. M. Agranovich, S. A. Darmanyan, and V. I. Rupasov, *Zh. Eksp. Teor. Fiz.* **78**, 656 (1980) [*Sov. Phys. JETP* **51**, 332 (1980)].

⁵M. S. Brodin, E. N. Myasnikov, and S. V. Marisova, *Polyaritonny v kristaloptike* (Polaritons in Crystal Optics), Naukova Dumka, Kiev, 1984.

- ⁶F. Askary and P. Y. Yu, *Solid State Commun.* **47**, 241 (1983); *Phys. Rev. B* **28**, 6155 (1983).
- ⁷V. V. Travnikov and V. V. Krivolanchuk, *Zh. Eksp. Teor. Fiz.* **85**, 2087 (1983) [*Sov. Phys. JETP* **58**, 1210 (1983)].
- ⁸V. M. Agranovich and V. L. Ginzburg, *Spatial Dispersion in Crystal Optics and the Theory of Excitons*, Springer, 1984, Chap. 3.
- ⁹V. M. Agranovich, in: *Surface Polaritons*, ed. by V. M. Agranovich and D. L. Mills, North-Holland, Amsterdam, 1982, p. 189.
- ¹⁰V. V. Katal'nikov and K. B. Tolpygo, *Fiz. Tverd. Tela (Leningrad)* **22**, 2928 (1980) [*Sov. Phys. Solid State* **22**, 1709 (1980)].
- ¹¹A. Bonnot and Benoît à la Guillaume, *Proc. First Taormina Res. Conf. Struct. Matter*, Pergamon, New York, 1974, p. 197.
- ¹²B. Sermage, M. Voos, and C. Schwab, *Phys. Rev. B* **20**, 3245 (1979).
- ¹³M. Yamawaki and C. Hamaguchi, *Phys. Status Solidi B* **112**, 201 (1982).
- ¹⁴V. E. Bisti, *Kratk. Soobshch. Fiz. No. 1*, 34 (1977).
- ¹⁵A. B. Pevtsov, S. A. Permogorov, A. V. Sel'kin, N. N. Syrbu, and A. G. Umanets, *Fiz. Tek. Poluprovodn.* **16**, 1399 (1982) [*Sov. Phys. Semicond.* **16**, 897 (1982)].
- ¹⁶A. V. Sel'kin, I. G. Stamov, N. N. Syrbu, and A. G. Umanets, *Pis'ma Zh. Eksp. Teor. Fiz.* **35**, 51 (1982) [*JETP Lett.* **35**, 57 (1982)].
- ¹⁷A. B. Pevtsov and A. V. Sel'kin, *Fiz. Tverd. Tela (Leningrad)* **23**, 2814 (1981) [*Sov. Phys. Solid State* **23**, 1644 (1981)].
- ¹⁸S. I. Pekar, *Zh. Eksp. Teor. Fiz.* **33**, 1022 (1957) [*Sov. Phys. JETP* **6**, 785 (1958)]; *ibid.* **34**, 1176 (1958) [7, 813 (1958)].
- ¹⁹J. J. Hopfield and D. G. Thomas, *Phys. Rev.* **132**, 563 (1963).
- ²⁰A. B. Pevtsov and A. V. Sel'kin, *Zh. Eksp. Teor. Fiz.* **83**, 516 (1982) [*Sov. Phys. JETP* **56**, 262 (1982)].
- ²¹A. V. Sel'kin, *Fiz. Tverd. Tela (Leningrad)* **19**, 1433 (1977) [*Sov. Phys. Solid State* **19**, 834 (1977)].
- ²²E. L. Ivchenko, A. B. Pevtsov, and A. V. Sel'kin, *Solid State Commun.* **39**, 453 (1981).
- ²³A. Ishimaru, *Wave Propagation and Scattering of Waves in Random Media*, Academic, 1980, Chap. 1, Part 9.
- ²⁴M. D. Galanin, E. N. Myanikov, and Sh. D. Khan-Magomedova, *Izv. Akad. Nauk SSSR Ser. Fiz.* **44**, 730 (1980).
- ²⁵G. N. Danilenko, M. Kh. Karapet'yants, V. E. Danilenko, and G. G. Magomedgadzhiev, *Dep. No. 3919-77*, VINITI, 1977.
- ²⁶V. M. Agranovich, *Teoriya eksitonov (Theory of Excitons)*, Nauka, Moscow, 1968, Part 2, Sec. 9.

Translated by S. Chomet